IX International Conference on Computational Methods for Coupled Problems in Science and Engineering
COUPLED PROBLEMS 2021
E. Oñate, M. Papadrakakis and B. Schrefler (Eds)

NUMERICAL MODELING OF FLOW AND STRAIN LOCALISATION IN PARTIALLY SATURATED POROUS MEDIA

M. ZAIM[*], G. SCIARRA[†], P. KOTRONIS[†] AND F. COLLIN[ς]

[*,†]Institut de recherche en génie civil et mécanique (GEM)
Ecole Centrale de Nantes (ECN)
1 Rue de la Noë, 44300 Nantes, France
e-mail: mohammed.zaim@ec-nantes.fr

[ς] Université de Liège/ArGenCo
Allee de la Decouverte, 9, 4000, Liège, Belgium
e-mail: f.collin@uliege.be

Key words: fingering, phase field, porous media, elasto-plastic, mixed finite element

Abstract. Coupling between fluid fingering and strain localization during the imbibition of a partially saturated soil is investigated in this paper. The fluid mixture saturating the granular skeleton is regarded as a non-uniform fluid characterized via a double well Helmoltz free energy endowed with a gradient regularizing contribution. The porous medium is assumed deformable and the associated elasto-plastic constitutive law is described by the "Sinfonietta Classica" plastic model. Because of the higher differential order of the hydraulic problem a mixed finite element method is employed.

1 INTRODUCTION

Fingering is a hydraulic instability that can occur in partially saturated porous media when a transversal perturbation of a fluid-fluid interface separating two fluids of different densities and viscosities progresses in time, see [1]. This can happen both during drainage and imbibition processes, say when a non-wetting fluid displaces a wetting one, initially saturating the porous medium, or viceversa when the wetting displaces the non-wetting fluid. The study of this phenomenon is of interest in several circumstances as the natural water infiltration of unsaturated soils, where air is the displaced phase, see e.g. [2, 3], or the sealing tightness of the caprock covering aquifer reservoir rocks used in underground gas storage or CO_2 sequestration applications, see e.g. [4].

As previously mentioned, both in the case of drainage and imbibition, fingering is induced by the loss of stability of a fluid front driven by a pressure gradient under transversal

perturbations. When this pressure gradient is due to gravity, gravity driven imbibition fingering occurs, see e.g. [5].

The typical approach based on the classical Richards equation [6], describing water infiltration through partially saturated soils, is definitely not suitable for capturing the structure of the fingering phenomenon, where the saturation degree is expected to localize in a narrow band. A purely hydraulic extension of the Richards model based on an enriched energy penalizing the gradient of the saturation degree, has been proposed in [7]. Alternatively modifications of the constitutive law of capillary pressure have been considered, which introduce a non-monotonic relation between the pore water pressure and the saturation degree, see e.g. [8], together with a regularization term depending on the rate of saturation as proposed in [9].

In this paper a phase field approach to partial saturation is adopted in the spirit of Landau and Cahn-Hilliard models, regarding the degree of saturation of the phase field parameter. Moreover the hydraulic model is inscribed within the framework of poromechanics in order to identify the effects of fingering instabilities on the strain and stress distribution in the porous skeleton. To do so an elasto-plastic model, retrieved from the literature, see e.g. [10], accounting for negative hardening induced by saturation, is adopted.

2 Phase field model for partially saturated porous media

The poromechanical model based on a phase field approach to partial saturation introduced in [11] is here adopted with the purpose of describing the formation of fingering instabilities and of possibly induced localized strains in a granular medium. The pore space is filled by a mixture of two phases, an incompressible liquid phase (water) and a gaseous phase (air) that is considered as passive, which means that its density can be neglected with respect to that of the liquid. The phase field approach consists to assume the gas-liquid mixture as a non-uniform fluid in the sense of Cahn-Hilliard [12] by introducing an order parameter, the phase field, which in this case is the saturation degree S_r.

Following the standard formulation of continuum poromechanics [13], the Lagrangian pull-back of the mass balance of this non-uniform fluid in the reference configuration of the solid skeleton can be written as follows:

$$\frac{dm_f}{dt} + \nabla.M = 0 \tag{1}$$

where $m_f = \rho_w \phi S_r$ is the mass of the mixture per unit reference volume, ϕ is the Lagrangian porosity, ρ_w the density of the liquid phase and M the mass flux.

The liquid and the gaseous phases of the non-uniform fluid are regarded as possible equilibrium states of the mixture. Therefore a double well potential describing the Helmoltz free energy of the fluid is introduced as a function of the saturation degree S_r:

$$\Psi_f(S_r) = C\frac{\gamma}{R}S_r^2(1-S_r)^2 \tag{2}$$

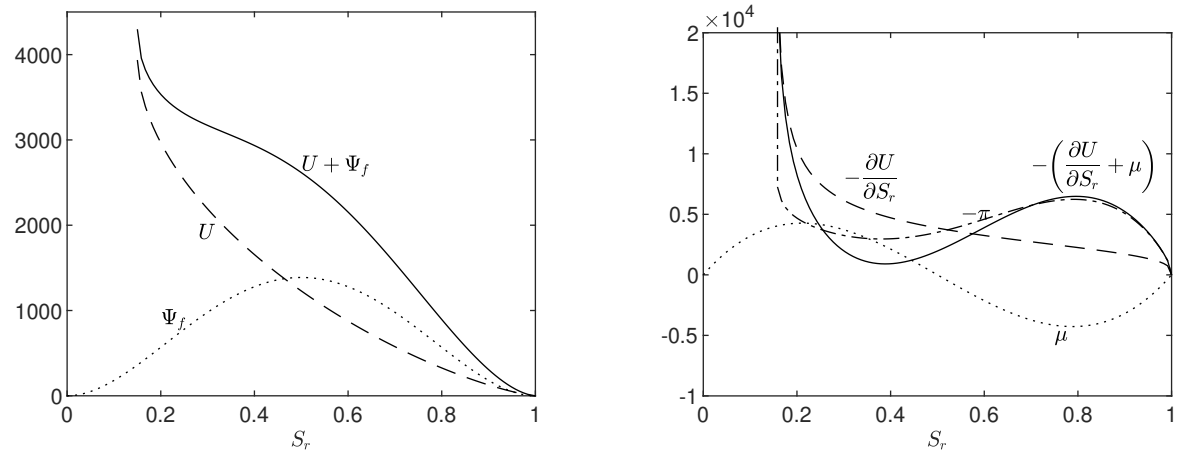

Figure 1: (a) Plot of the energy of the non-uniform fluid Ψ_f, the capillary energy U and the energy of the pore fluid mixture $\Psi_f + U$; (b) plot of the corresponding first order energy derivatives, μ, $-\partial U/\partial S_r$, $s = -\mu - \partial U/\partial S_r$ and $-\pi(S_r)$

As depicted in Figure 1 the two minima of Ψ_f correspond to the zeros of its non-monotonic first derivative $\mu = \partial \Psi_f / \partial S_r$, which physically represents the chemical potential of the fluid, where the fluid mass moves from higher to lower potentials.
In equation (2), γ is the liquid-gas surface tension and R a characteristic length describing the effective size of the pore space through which the fluid can flow; in the following the Leverett estimate of R is considered $R = \sqrt{\frac{\varkappa}{\phi_0}}$, ϕ_0 being the initial porosity and $\varkappa$ the intrinsic permeability.
As the fluid mixture just occupies the porous network of the granular skeleton, following [11] we consider from now on an additional contribution to the pore fluid energy accounting for the retention properties of the solid skeleton. This is the classical capillary energy which can be prescribed via a vanGenuchten formulation so that its derivative is given by

$$\frac{\partial U}{\partial S_r} = -(\rho_w g)\frac{1}{\alpha}\left[\left(\frac{S_r - S_r^{res}}{1 - S_r^{res}}\right)^{\frac{-1}{m}} - 1\right]^{\frac{1}{n}} \tag{3}$$

where α is the inverse of the capillary rise and S_r^{res} is the liquid residual saturation.
The energy and the chemical potential of the pore fluid, say of the non-uniform fluid within the porous network, differ therefore from those of the pure mixture, see Figure 1. The coefficient C of equation (2) gives the relative weight of the mixture free energy with respect to the capillary one.

In order to convexify the problem a gradient contribution to the free energy of the non-uniform fluid is finally added as

$$\Psi_{nl} = \frac{1}{2} c \nabla(\phi S_r) \nabla(\phi S_r) \tag{4}$$

which allows to incorporate in the model a penalization associated to the diffuse interface formation. In equation (4) c is an higher order stiffness incorporating the notion of a characteristic length ℓ corresponding to the square root of the ratio between c and $\rho_w g \alpha^{-1}$.

The variational derivative of the overall pore fluid energy accounting for the contributions of Ψ_f, U and Ψ_{nl} provides the expression of the so called effective chemical potential, therefore defined as follows

$$\mu^{eff} = \frac{\partial U}{\partial S_r} + \frac{\partial \Psi_f}{\partial S_r} - \left(\frac{\partial \Psi_{nl}}{\partial (\phi S_r)_{,l}} \right)_{,l} \tag{5}$$

In the framework of this enriched poromechanical model the mass flux M is described by a generalized Darcy's law:

$$M_k = -\rho_w \frac{\varkappa k(S_r)}{\eta} (\mu^{eff}_{,k} - \rho_w g_k) \tag{6}$$

where $k(S_r)$ is a function that accounts for non-uniform mobility of the fluid mixture within the pore network, from now on assumed to coincide with the relative permeability of the liquid phase ($k(S_r) = S_r^3$), η being the viscosity of the liquid.

Replacing equation (5) into equation (6) and this last into the fluid mass balance (1) implies the following fourth order partial differential equation for the saturation degree:

$$\frac{d\phi S_r}{dt} = \left\{ \frac{\varkappa k(S_r)}{\eta} \left[\left(\frac{\partial U}{\partial S_r} + \frac{\partial \Psi_f}{\partial S_r} - \left(\frac{\partial \Psi_{nl}}{\partial (\phi S_r)_{,l}} \right)_{,l} \right)_{,k} - \rho_w g_k \right] \right\}_{,k} \tag{7}$$

In addition to the mass balance equation, the momentum balance equation of the porous medium must be also considered, say

$$div(\sigma) + f = 0 \tag{8}$$

where f is the body force and σ is the total stress defined following [13] as $\sigma = \sigma' - b\pi(S_r)1$, with σ' the effective stress, b the Biot coefficient and $\pi(S_r) = S_r \partial(U + \Psi_f)/\partial S_r - (U + \Psi_f)$ the equivalent pore pressure, see Figure 1.

3 The elasto-plastic constitutive model

The constitutive relation for the effective stress is provided via an elasto-plastic constitutive model where, for the sake of simplicity, the elastic part is kept as the classical Hooke law, while the plastic one is assumed to be given via a non-associate plastic model introduced in the eighties by Nova: the Sinfonietta Classica model [14]. Let $p' = -\frac{Tr(\sigma')}{3}$ be the effective pressure and $q' = \sqrt{\frac{3}{2} s' : s'}$ the deviator stress defined as the second invariant of the deviatoric (effective) stress $s' = \sigma' + p'1$. The yield function f and the plastic potential g are given by:

$$f = 3\beta(\iota - 3) \ln \frac{p'}{p_c} + \frac{3}{2}(\iota - 1) \frac{q'^2}{p'^2} + 3\iota \frac{det(s')}{p'^3} = 0 \tag{9}$$

$$g = 9(\iota - 3)\ln\frac{p'}{p_g} + \frac{3}{2}(\iota - 1)\frac{q'^2}{p'^2} + 3\iota\frac{det(s')}{p'^3} = 0 \tag{10}$$

where β controls the associativity of the plastic law, it can be observed that the normality rule applies only if $\beta = 3$. The parameter ι is defined by $\iota = (9 - Z^2)/(3 - Z^2 + 2Z^3/9)$ where Z indicates the slope of the characteristic state line: $Z = 6\sin\varphi/(3 - \sin\varphi)$, φ being the friction angle and p_c is the so-called preconsolidation pressure, say the highest mean effective stress ever experienced by the granular medium.

Depending on the values of the β and ι the model allows to characterize the behavior of materials ranging from sands to soft rocks, especially during monotonic loading.

Following [10] a double hardening law is introduced for the preconsolidation pressure which separately accounts for the parametrization of $\dot{p}_c$ by the plastic strain rate as well as by the variation of the saturation degree:

$$\dot{p}_c = \dot{p}_{c(sat)} + \dot{p}_{c(unsat)} \tag{11}$$

where $\dot{p}_{c(sat)}$ is given by the original Sinfonietta Classica hardening law

$$\dot{p}_{c(sat)} = \frac{p_c}{\beta_p}\left(- \dot{\varepsilon}^p_v + \chi\sqrt{\dot{\varepsilon}^p_d : \dot{\varepsilon}^p_d}\right) \tag{12}$$

with $\dot{\varepsilon}^p_v = Tr(\dot{\varepsilon}^p)$ and $\dot{\varepsilon}^p_d = \dot{\varepsilon}^p - \frac{1}{3}\dot{\varepsilon}^p_v 1$ the volumetric and the deviatoric parts of the plastic strain rate and $\dot{p}_{c(unsat)}$ describes the variation of the preconsolidation pressure with respect to the variation of the saturation degree:

$$\dot{p}_{c(unsat)} = -\lambda p_c \dot{S}_r \tag{13}$$

In equation (13) λ is a constitutive parameter to be calibrated.

4 Modeling fluid fingering instabilities and coupled strains during imbibition

4.1 Numerical procedure

The coupled problem described by the mass balance equation (7) and the momentum balance equation (8) endowed with the constitutive law of the generalized chemical potential and the total and effective stress is solved numerically using the finite element method. In order to reduce regularity of shape functions needed to solve equation (7) a mixed finite element approach is adopted building up a weak coupled formulation for the two coupled second order differential equations (1) and (5) prescribing the evolution of the saturation degree and the generalized chemical potential. As a consequence both S_r and μ^{eff} are going to be regarded in the following as nodal unknowns.

The time derivative in the fluid mass balance is discretized adopting an implicit Euler scheme. Due to the non-linearity of the problem with respect to the plastic strain and the degree of saturation a nested Newton-Raphson method is developed in order to resolve the

plastic constitutive law in the Gauss points and to calculate the saturation degree, together with the generalized chemical potential and the displacement of the porous medium in all the nodes of the finite element discretization. The model was implemented in a Matlab finite element code [15] allowing in its original version to solve non-linear mechanical problems.

4.2 Problem Set-Up

We simulate water infiltration into an initially partially saturated and initially confined loamy sand in plane strain conditions. The domain is a $1 \times 0.6\ m^2$ rectangle. The mesh is made of 15748 unstructured linear triangular finite elements generated by Gmsh [16]. The element size is half the intrinsic length ℓ, assumed as $\ell = 0.01L$, L being the characteristic size of the domain. The soil is assumed homogeneous and isotropic. The model parameters are summarized in Table 1.

The initial saturation is $S_r^0 = 0.2$ while the initial confinement is given by a pressure of $400KPa$. Starting from this initial state we set the displacement to zero and we keep the stress state then we apply a vertical downward oriented inflow at the top surface of the domain, while at the bottom surface the generalized chemical potential remains constant and equal to its initial value.

Boundary conditions are reported in Table 2.

Table 1: Model parameters

	Parameter	Value	Unit
Young modulus	E	4340	KPa
Poisson's ratio	ν	0.36	-
Biot coefficient	b	0.79	-
Friction angle	φ	36	$^\circ$
Permeability	$\varkappa$	10^{-12}	m^2
Saturated permeability	K_{sat}	10^{-5}	m/s
	β	3	-
	β_p	0.01	-
	λ	2	-
Initial preconsolidation pressure	p_c^0	500	KPa
Initial porosity	ϕ_0	0.37	-
Water density	ρ_w	1000	Kg/m^3
Water viscosity	η	0.00089	$Pa.s$
Residual saturation	S_r^{res}	0.1567	-
	α	3.52	m^{-1}
	n	3.17	-

Table 2: Boundary conditions for the incremental problem

	Top surface	Bottom surface	Right surface	Left surface
Mechanical	$\sigma \cdot n = 0$	$u_x = 0$ $u_y = 0$	$\sigma \cdot n = 0$	$\sigma \cdot n = 0$
Hydraulic	$S_r = 0.85$ $q \cdot n = -0.1 K_{sat}$	$\mu^{eff} = -3.79 KPa$	$q \cdot n = 0$	$q \cdot n = 0$

4.3 Results

In this section the results of the gravity driven imbibition process are presented analyzing and comparing, in particular, the occurrence of fingering instabilities, exhibited by the saturation degree, with the evolution of the plastic strain induced by saturation.

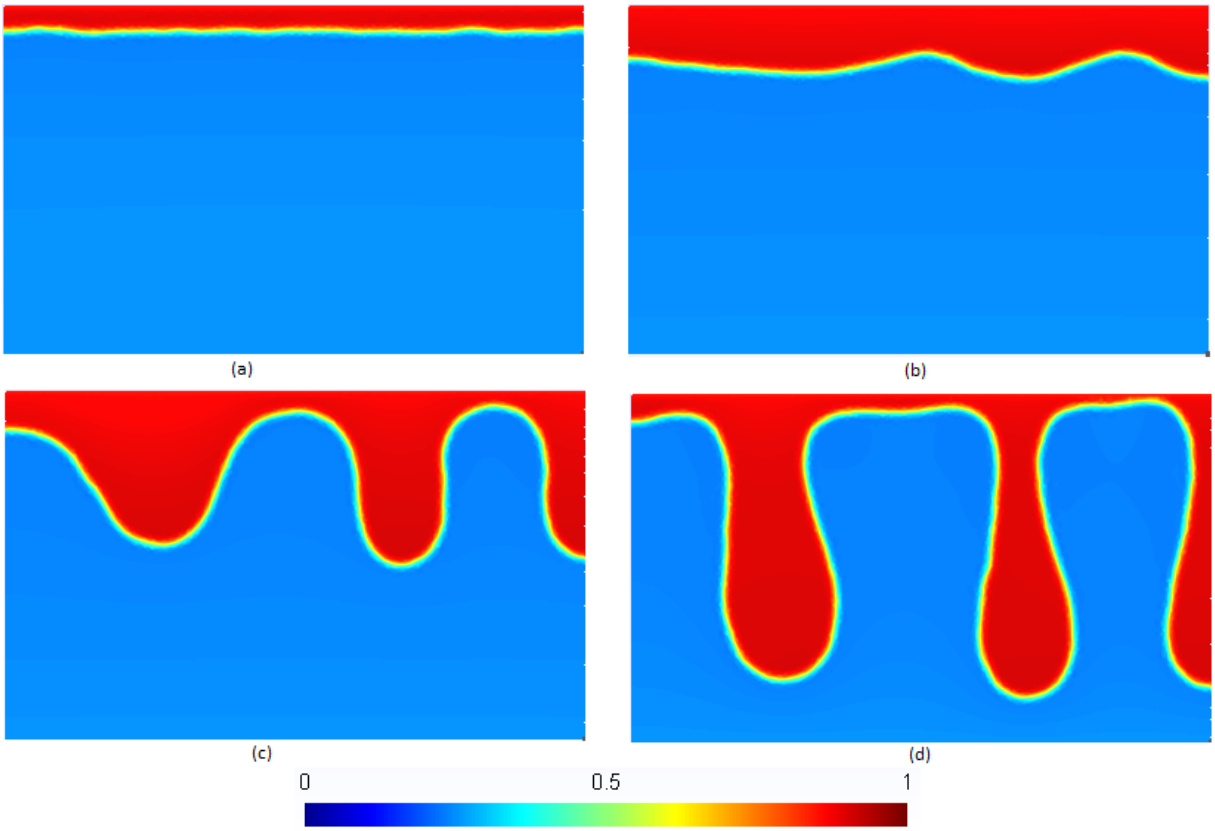

Figure 2: The distribution of water saturation at different times. (a) $t = 8000s$. (b) $t = 22000s$. (c) $t = 32000s$. (d) $t = 40000s$

The four panels of Figure 2 show the space and time evolution of S_r within the granular medium. A downward moving liquid front forms, panel (a), and progressively destabilized,

panel (b), exhibiting almost periodic transversal oscillations. Fingers start to form, panel (c), and propagate towards the bottom of the sample. Withdrawal of the liquid phase is observed close to the injection point, panel (d). A relatively small overshoot can be observed in panel (d) behind the tip of the finger.

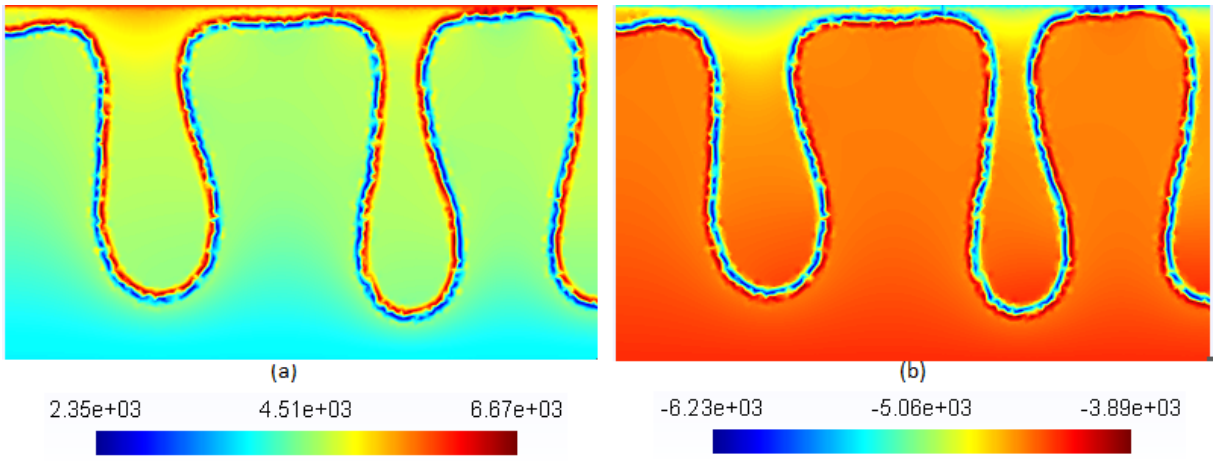

Figure 3: (a) The plot of the generalized capillary pressure $s = -\mu - \partial U/\partial S_r$; (b) The plot of the equivalent pore pressure $\pi(S_r) = S_r \partial(U + \Psi_f)/\partial S_r - (U + \Psi_f)$

In Figure 3a the plot of the generalized capillary pressure $s = -\mu - \partial U/\partial S_r$ is reported. The S-shaped profile of s, at the interface between the finger and the almost dry material, is apparently due to the non-monotonic behavior of s as a function of S_r. This implies the generalized capillary pressure to reduce in the more external part of the diffuse interface, then to grow and reduce again when following a transversal section of the finger, see also Figure 7. The small overshoot in the profile of S_r is responsible for a similar oscillation of s behind the tip of the finger. In Figure 3b the profile of the equivalent pore pressure, π is also reported, which exhibits a similar behavior as that of s.

In Figure 4 the plot of the effective chemical potential μ^{eff}, panel (a), and of the second gradient contribution $-c\nabla \cdot \nabla(\phi S_r)$ to it, panel (b), are drawn. It is worth to notice that no significant concentration in the μ^{eff} profile can be observed at the interface between the dry and the wet zone, this because the second gradient contribution definitely counterbalances the effect of the generalized capillary pressure through the interface.

The negative hardening, described by equation (13), which is induced by the progressive saturation of the sample, implies that an initially elastic state of stress can become plastic just because of the shrinkage of the reversibility domain. Plastic strains therefore naturally arise allowing the effective stress to remain almost constant during the wetting process, see Figure 5. Because of biaxial loading conditions the initial state of stress is definitely non-isotropic which therefore implies the plastic strains to have volumetric and deviatoric components different from zero.

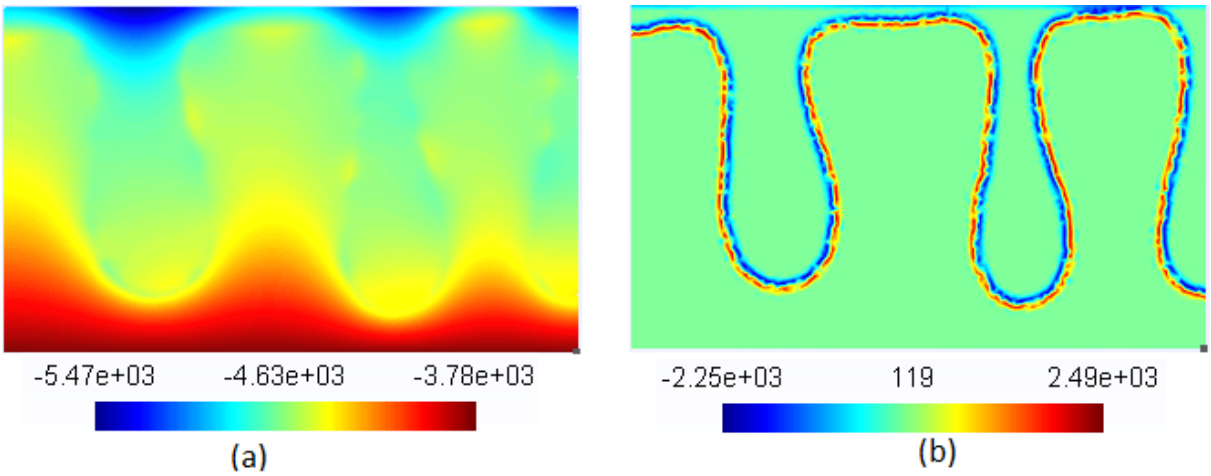

Figure 4: (a) The plot of the effective chemical potential μ^{eff} at $t = 40000s$. (b) The plot of the second gradient term $c\nabla.\nabla(\phi S_r)$ at $t = 40000s$

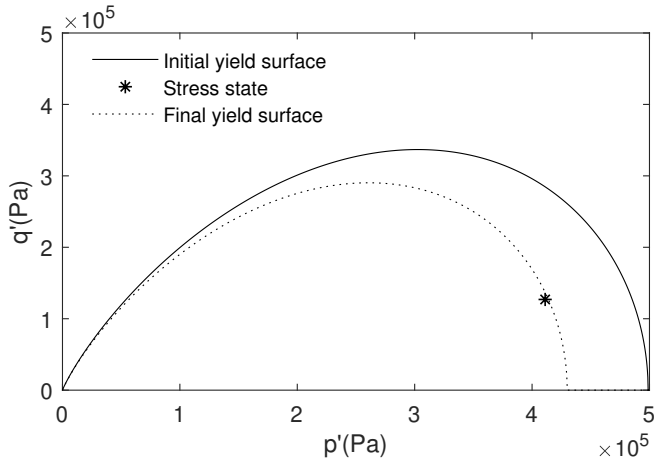

Figure 5: Plots of the initial yield surface, the stress state and the final yield surface in (p', q') plane

The space and time evolution of the volumetric plastic strain is reported in Figure 6. Looking at the first three panels it can be observed that plastic strains appear in a region when the saturation front passes through it. This behavior is detailed in Figure 7 comparing the two profiles of S_r and ϵ_v^p at a time $t = 40000s$. It is evident that the diffuse interface between the dry and the wet region includes the one between the elastic and the plastic zone. The widthness of this overlapping being correlated to the value of the coefficient λ describing the negative hardening.

Comparing panels (c) and (d) of Figure 2 and Figure 6 it is interesting to remark that the fingering in the saturation degree do not coincide with those of the plastic strain after withdrawal of water. This is obvious because of the irreversibility of the plastic strains.

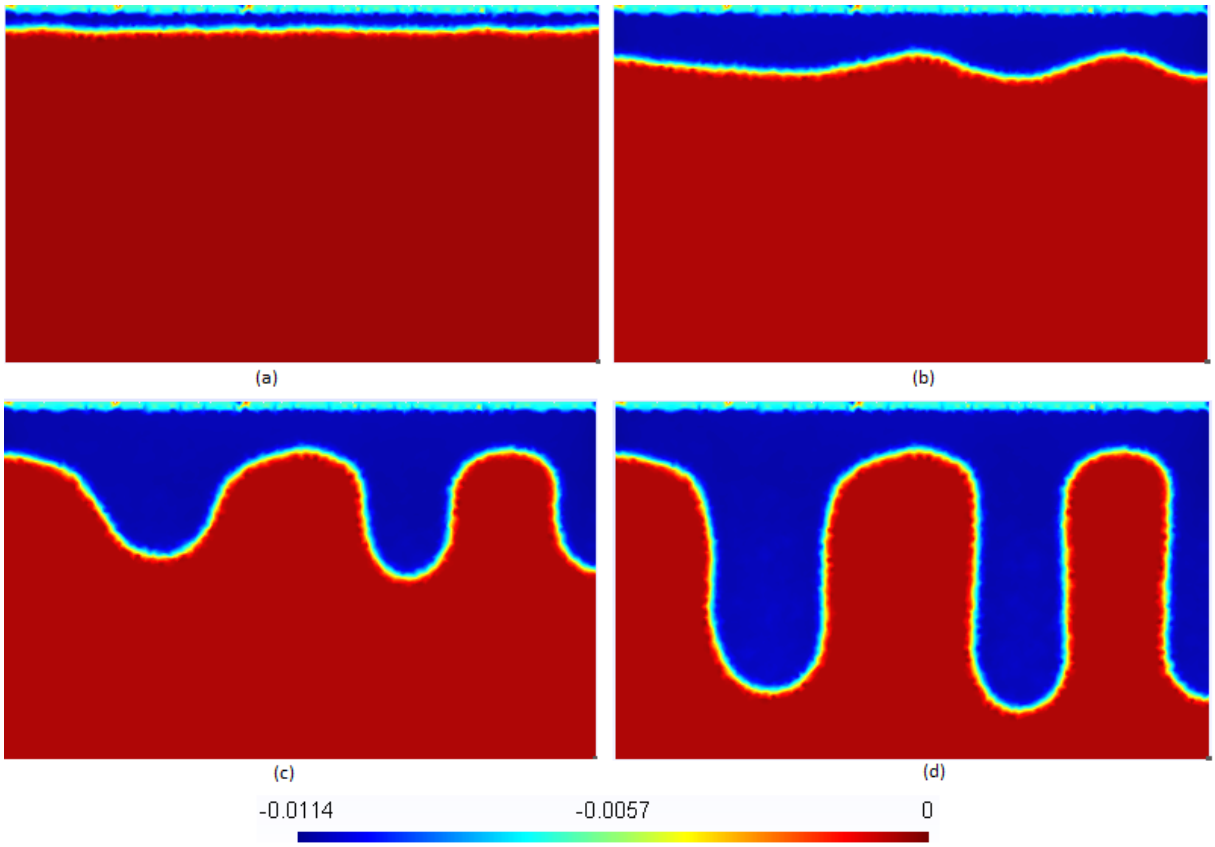

Figure 6: The volumetric plastic strain ε_v^p at different times. (a) $t = 8000s$. (b) $t = 22000s$. (c) $t = 32000s$. (d) $t = 40000s$

As for the total volumetric strain, this last shows a slightly growing profile along the mean section of the finger, with respect to that of the plastic volumetric strain, see Figure 7. This is due to the above mentioned small overshoot of the degree of saturation and to the poroelastic stress-strain relation.

Finally the contour plot of the deviatoric plastic strain, panel (a), and the deviatoric total strain, panel (b), are shown in Figure 8. As the shape of the fingers reflects those of the volumetric plastic strain it is interesting to remark that the total deviatoric strain concentrates in the zones of withdrawal of the liquid phase as well as at the tip of the finger, while inside it is almost vanishing. The comparison between the plastic and the total deviator strain plots indicates that the elastic component of the deviatoric strain definitely compensate plastic effects inside the finger and become dominant in the high curvature zones of the finger profile.

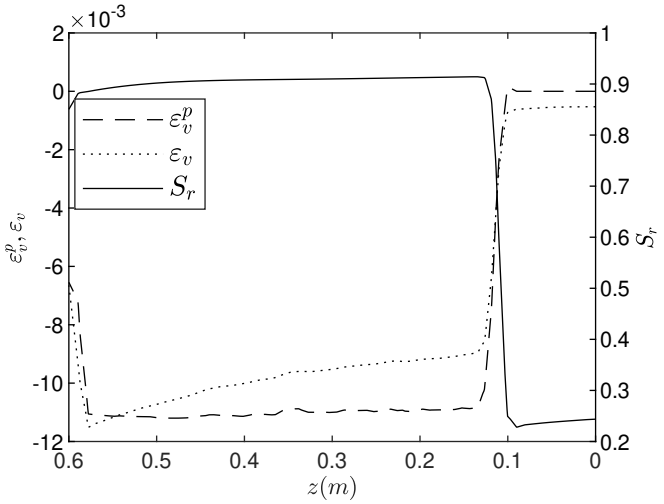

Figure 7: Plots of the saturation degree S_r, the total volumetric strain ε_v and the volumetric plastic strain ε_v^p at a time $t = 40000s$ along a finger section

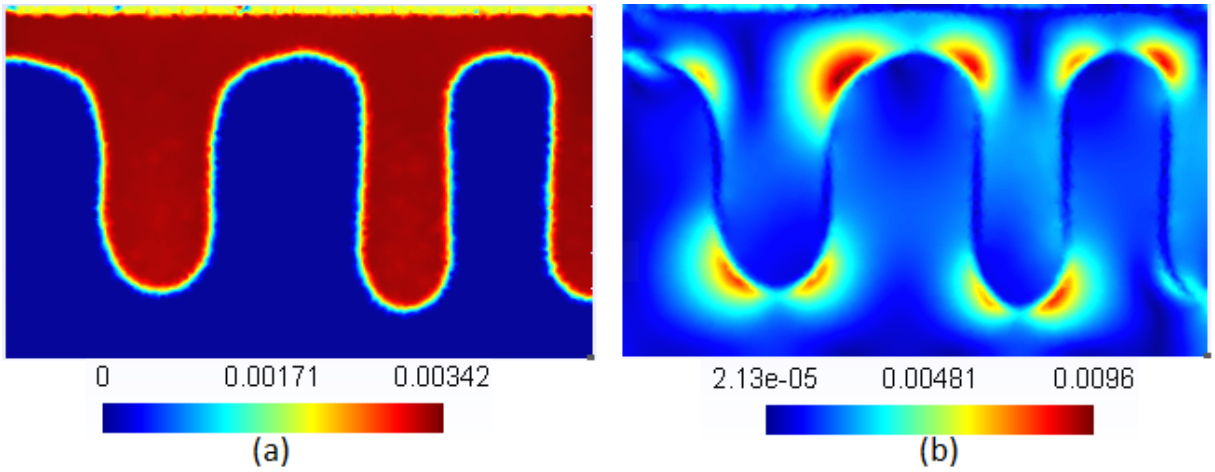

Figure 8: (a) Deviatoric plastic strain at t=40000s. (b) Total deviatoric strain at t=40000s

5 CONCLUSIONS

In this paper, we have presented a poromechanical model based on a phase field approach that describe fingering formation during water infiltration into an initially dry soil. An elasto-plastic constitutive model extended to include the effect of the variation of the saturation degree on the hardening law has been adopted to describe the response of the granular material during water infiltration process.

Concerning hydraulic response, the space and time evolution of the saturation degree within the granular medium show the formation of fingers. Moreover the hydro-mechanical coupling has been analyzed through the space and time evolution of the volumetric and

the deviatoric plastic strain. A maximum plastic deformation due to the shrinkage of the yield surface appears in a subdomain when the saturation front passes through it.

REFERENCES

[1] P. G. Saffman and G. I. Taylor, "The penetration of a fluid into a porous medium or hele-shaw cell containing a more viscous liquid," *Proceedings of the Royal Society of London. Series A. Mathematical and Physical Sciences*, vol. 245, no. 1242, pp. 312–329, 1958.

[2] L. Cueto-Felgueroso and R. Juanes, "A phase field model of unsaturated flow," *Water resources research*, vol. 45, no. 10, 2009.

[3] L. Cueto-Felgueroso, M. J. Suarez-Navarro, X. Fu, and R. Juanes, "Numerical simulation of unstable preferential flow during water infiltration into heterogeneous dry soil," *Water*, vol. 12, no. 3, p. 909, 2020.

[4] J. Rutqvist, "The geomechanics of co 2 storage in deep sedimentary formations," *Geotechnical and Geological Engineering*, vol. 30, no. 3, pp. 525–551, 2012.

[5] D. A. DiCarlo, "Experimental measurements of saturation overshoot on infiltration," *Water Resources Research*, vol. 40, no. 4, 2004.

[6] L. A. Richards, "Capillary conduction of liquids through porous mediums," *Physics*, vol. 1, no. 5, pp. 318–333, 1931.

[7] A. Beljadid, L. Cueto-Felgueroso, and R. Juanes, "A continuum model of unstable infiltration in porous media endowed with an entropy function," *Advances in Water Resources*, vol. 144, p. 103684, 2020.

[8] D. A. DiCarlo, R. Juanes, T. LaForce, and T. P. Witelski, "Nonmonotonic traveling wave solutions of infiltration into porous media," *Water resources research*, vol. 44, no. 2, 2008.

[9] S. M. Hassanizadeh, M. A. Celia, and H. K. Dahle, "Dynamic effect in the capillary pressure–saturation relationship and its impacts on unsaturated flow," *Vadose Zone Journal*, vol. 1, no. 1, pp. 38–57, 2002.

[10] R. Tamagnini, "An extended cam-clay model for unsaturated soils with hydraulic hysteresis," *Géotechnique*, vol. 54, no. 3, pp. 223–228, 2004.

[11] G. Sciarra, "Phase field modeling of partially saturated deformable porous media," *Journal of the Mechanics and Physics of Solids*, vol. 94, pp. 230–256, 2016.

[12] J. W. Cahn and J. E. Hilliard, "Free energy of a nonuniform system. i. interfacial free energy," *The Journal of chemical physics*, vol. 28, no. 2, pp. 258–267, 1958.

[13] O. Coussy, *Poromechanics*. John Wiley & Sons, 2004.

[14] R. Nova, "Sinfonietta classica": a strain-hardening model for soils and soft rocks," 2001.

[15] d. M. Bonnet and A. Frangi, "Analyse des solides déformables par la méthode des éléments finis," *European Journal of Computational Mechanics/Revue Européenne de Mécanique Numérique*, vol. 16, no. 5, pp. 667–668, 2007.

[16] C. Geuzaine and J.-F. Remacle, "Gmsh: A 3-d finite element mesh generator with built-in pre-and post-processing facilities," *International journal for numerical methods in engineering*, vol. 79, no. 11, pp. 1309–1331, 2009.